Strain localization in sandstone and its implications for CO_2 storage

A. Torabi[1*], R.H. Gabrielsen[2], H. Fossen[3], P. Ringrose[4, 5], E. Skurtveit[6], E. Ando[7], F. Marinelli[8], G. Viggiani[7], S. Dal Pont[7], A. Braathen[2], A. Hovland[1], P. Bésuelle[7], R. Alikarami[1], H. Zalmstra[2] and D. Sokoutis[2, 9] explore how rock strain influences fluid communication and how structural architecture might affect CO_2 storage effectiveness.

Introduction

Geological storage of CO_2 is a key technical solution to the climate-energy challenge, but it has a number of technological constraints (Baines and Worden 2004; Halland et al., 2011), broadly under the themes of assuring adequate storage capacity and long-term storage integrity. A suitable CO_2-storage reservoir should consist of rock formations with sufficient porosity, permeability and connectivity in order to provide an adequate storage volume. The role of faults and their associated deformation structures (such as deformation bands and fractures) in controlling both storage capacity and long-term storage integrity is thus a key factor in achieving globally significant CO_2 storage (Figure 1).

Although some sedimentary basins on the Norwegian continental shelf already harbour operational CO_2-injection and storage projects such as Sleipner (Zweigel et al., 2004) and Snøhvit (Hansen et al., 2013), our understanding of reservoir fluid communication due to compartmentalization is far from complete and will be important for further use of the offshore basins for CO_2 storage. In addition to the inherited structural features, elevated injection pressures may cause hydraulic fractures or stimulate fault reactivation which both point to the need to characterize the geomechanical response of the rock system to CO_2 injection (Rutqvist, 2012; Iding and Ringrose, 2010). In the present work, we investigate the effects of faults and their related structures on the geomechanical and petrophysical properties of sandstone reservoirs. Important components of fault systems include fractures and deformation bands in the damage zone and fault core (Caine et al., 1996; Shipton and Cowie, 2003; Fossen et al., 2007). Fault systems may enhance or suppress fluid communication, which in turn may affect the storage capacity and conductivity of the candidate reservoirs (Figure 1).

As a case study, a reservoir model of the Tubåen Formation at the Snøhvit CO_2 injection site in the Barents Sea (Grude et al., 2013; Hansen et al., 2013) was investigated using 4D seismic data and fault attribute analysis. The characteristics of deformation structures (e.g. sub-seismic faults, deformation bands and fractures) were investigated by field studies of outcrop analogues and by triaxial laboratory experiments to provide a basis for numerical modelling. Fault architecture within reactivated fault systems was studied by the use of analogue modelling. Key questions addressed in the work include: a) Where and when might strain localize in the reservoir? b) How does rock strain influence fluid communication? c) How might structural architecture affect CO_2 storage effectiveness?

Strain localization in sandstone and the related flow properties

Faults can provide good seals, retaining large columns of oil or gas over millions of years. However, under varying conditions of applied stress or elevated pore pressures, faults may become efficient conduits for fluid flow along and across them with flow rates up to ~1-10 m/day (Figure 1). It is therefore of vital importance to understand the fault architecture and the process of strain localization and faulting in sandstone in order to evaluate potential storage sites.

The macroscopic properties of larger fault systems are controlled by fault separation, characteristics of fault rocks (including the effects of clay smear and fault smear), and the effects of tectonic reactivation (Hildebrand and Kroon, 2003; Gray et al., 2012; Couples, 2005; Yielding et al., 2011). Such structural elements may affect both the caprock and the reservoir rock (Figure 1).

[1] *Uni Research CIPR, Allegate 41, 5007 Bergen, Norway.*
[2] *University of Oslo, Sem Sælands vei 1, 0371 Oslo, Norway.*
[3] *University of Bergen, Allegate 41, 5007 Bergen, Norway.*
[4] *Statoil ASA, 7005 Trondheim, Norway.*
[5] *Norwegian University of Science and Technology, 7491 Trondheim, Norway.*
[6] *Norwegian Geotechnical Institute, Postboks 3930 Ullevål Stadion, 0806 Oslo, Norway.*
[7] *Univ. Grenoble Alpes, 3SR, 38000 Grenoble, France.*
[8] *Northwestern University, 2145 Sheridan Road, Tech A333, Evanston, IL 60208-3109 , USA.*
[9] *Universiteit Utrecht, Budapestlaan 4, 3584 CD Utrecht, Netherlands.*
[*] *Corresponding author, E-mail: anita.torabi@uni.no*

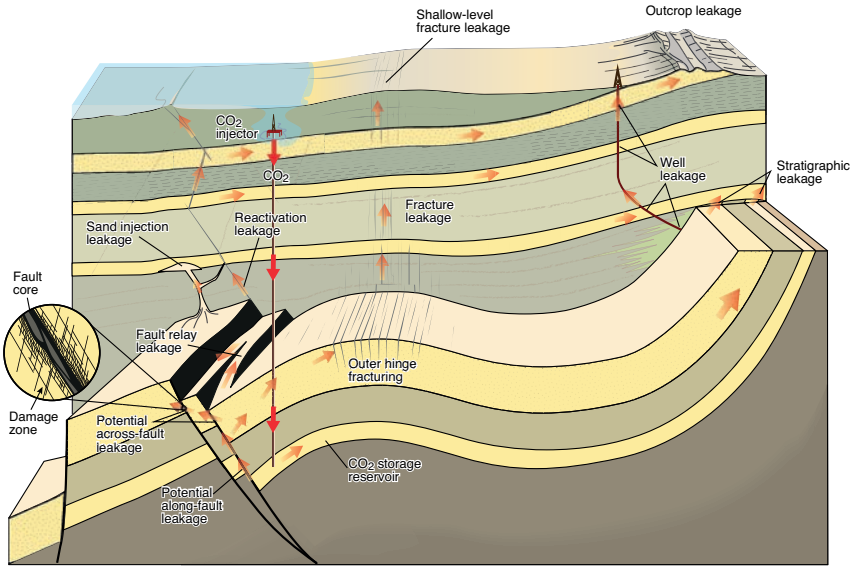

Figure 1 *Generalized illustration of subsurface structures relevant for identifying possible CO_2-leakage pathways.*

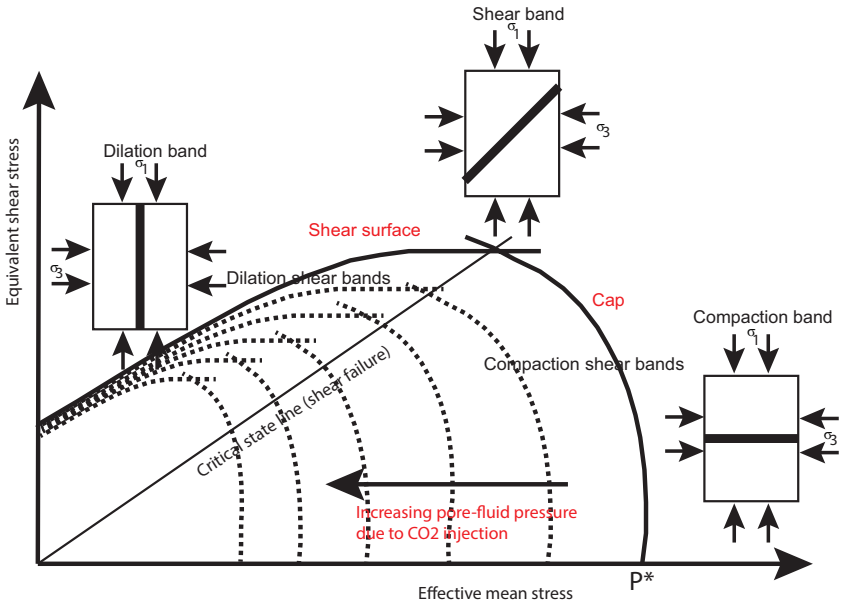

Figure 2 *A modified Cam-Clay model for porous sandstone, which includes two yield surfaces, a shear surface and a cap. Different deformation modes (dilation, shear, and compaction) occur in the conditions that are met along the yield surfaces. Note the effect of pore-pressure change on the model.*

Fractures and deformation bands can have a wide range of effects on fluid flow, both promoting and suppressing fluid communication. Kinematically, deformation bands can be classified as one of three end members (Fossen et al., 2007) or combinations thereof, namely dilation bands, compaction bands, and shear bands. Among deformation bands, cataclastic bands (which involve crushing, shear and compaction of the grains) are the most common and can significantly alter the petrophysical properties of the reservoirs (e.g. Torabi et al., 2013).

Usually, granular materials such as porous sandstones respond to stress by volumetric changes, which are not taken into account by the failure criteria developed for brittle rocks (such as Mohr-Coulomb). More sophisticated yield criteria and mechanical models such as the Drucker-Prager criterion and the modified Cam-Clay Cap model (e.g. Bésuelle and Rudnicki, 2004) are needed to predict different deformation modes in porous sandstone reservoirs under different stress conditions. The modified Cam-Clay Cap model uses a plot of shear stress versus mean stress to describe two yield surfaces, a shear surface and a compaction surface (Cap), which allows for a complete analysis of deformation modes in porous sandstone from dilation to shear and compaction (Figure 2). The condition for faulting is satisfied on the critical state line, which intersects the shear surface at the maximum shear stress. Pore pressure increase (e.g. due to CO_2-injection) and uplift of the sediments (unloading) reduce the effective mean stress and the stress state moves closer to critical pressure for failure (Figure 2). It is therefore crucial to predict the deformation behaviour of rocks and the optimal pressure change that they can sustain when evaluating and assessing risk for CO_2-injection in such reservoirs.

Analytical methods and data analysis

Seismic interpretation and attribute analysis of faults in the Snøhvit Field

By combining seismic interpretation calibrated to wells, and seismic attribute analysis (e.g. Chopra and Marfurt, 2008; Henderson, 2012), we identify geological heterogeneities that may influence CO_2 storage at the Snøhvit site. Two 3D reflection seismic data sets used in this study were acquired in 2003 (before injection), and in 2009 (after injection). The surveys cover an area of 8 km x 8 km around the injection well (7121/4F2H) at the Snøhvit site (Figure 3b). The structure of the field is dominated by an E-W-trending horst-and-graben-system. This fault system is terminated towards the deep Bjørnøya Basin to the west by the N-S-trending down to the west extensional Ringvassøy-Loppa Fault Complex (Gabrielsen et al., 1997; Figure 3). The Snøhvit Field can be structurally divided into a main segment and a F-segment (Hansen et al., 2011). A relay ramp bridges the two segments. The CO_2-injection-well is located in the F-segment, where the CO_2 was injected into Tubåen Formation (Figure 3c).

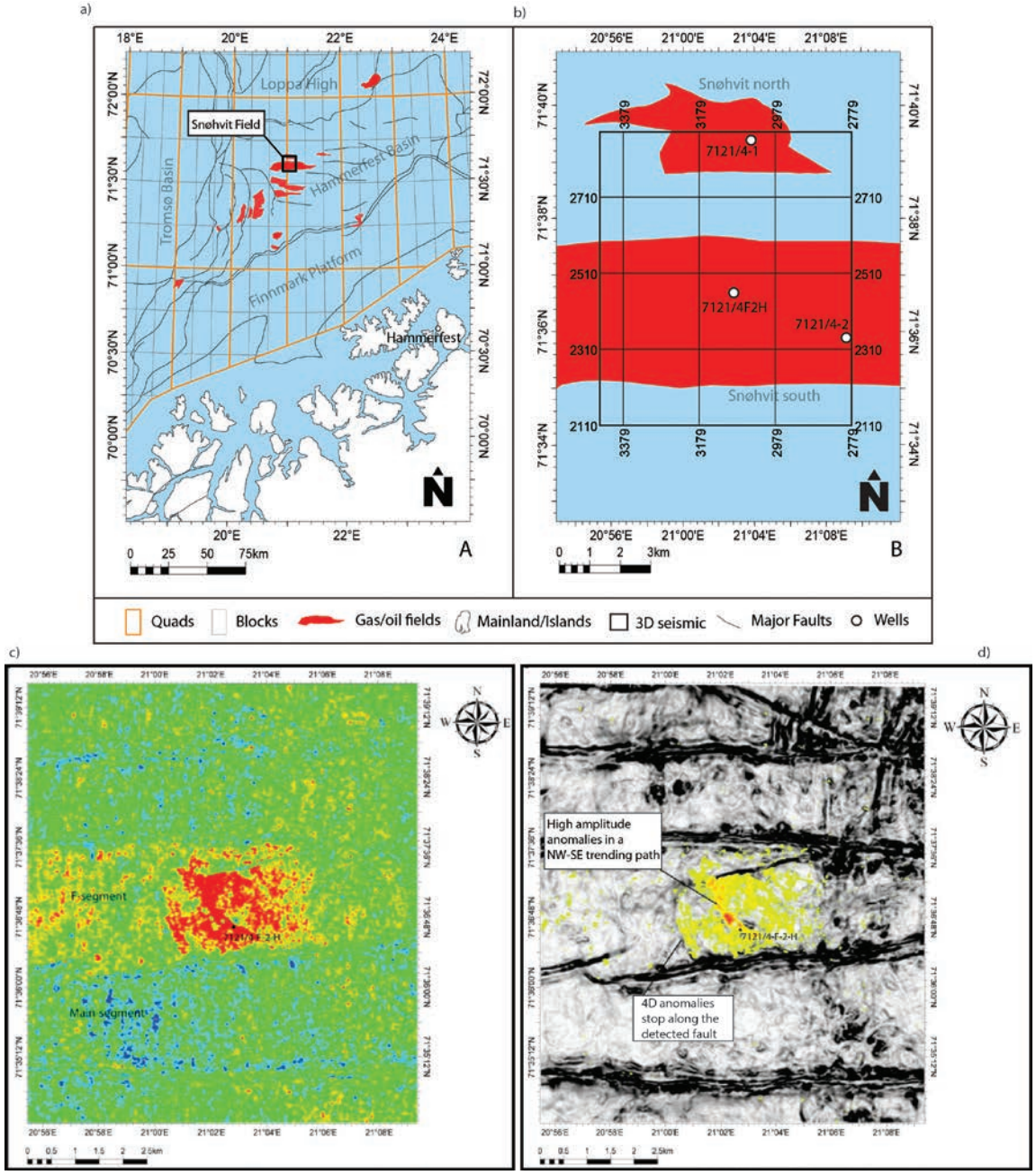

Figure 3 *a) Map of the studied area with the main structural elements of the Hammerfast Basin. b) Map of Snøhvit Field with well locations (After Hovland, 2013; modified from NPD Fact Maps).c) Envelope attribute difference of injection interval before and after CO_2 injection, d) Extracted semblance map superimposed by the 4D anomalies (after Hovland, 2013).*

A series of surface and volume attributes were applied to investigate the structural elements as well as the influence of injected CO_2 on seismic amplitude response. Firstly, an advanced fault imaging workflow (Hovland, 2013) was used to provide high-resolution fault attribute volumes. The large-scale fault detection attribute analysis was used to identify the major faults with a high confidence level and also several previously undetected potential faults with a medium confidence inside different fault blocks. The small fault detection attribute identified many low confidence small-scale faults within the fault blocks. Such anomalies are known to influence the CO_2-migration.

Using a second workflow (Hovland, 2013), envelope attributes of the CO_2 storage reservoir interval before and after injection showed a significant amplitude anomaly which is caused by CO_2 injection (Figure 3). By co-blending amplitude and fault attributes we visualized several structures, among them a NW-SE trending structure that appears within the F-segment, which seems to have acted as a pressure barrier (Figure 3d). To the west of the injection well, the 4D anomalies (envelope attribute difference) stop rather abruptly against a detected structure (Figure 3d). Judging from the variance map, the structure is most likely a N-S trending accommodation-fault, although a stratigraphic barrier is also possible. Other studies (Hansen et al., 2011; Chiaramonte et al., 2014) have shown that such barriers have controlled the pressure response at the Snøhvit CO_2 injection site and are critical to understanding the storage integrity.

Deformation of high porosity and low porosity sandstones (field study)

Deformation in sandstone can occur in the form of deformation bands and/or fractures, depending on the porosity and degree of lithification (e.g., Fossen et al., 2007), with fractures dominating in tighter sandstones (porosity < 12%). For CO_2 storage in sandstone reservoirs, differential stress, CO_2 fluid pressure and CO_2-brine reactions causing dissolution of load-carrying framework minerals could change the failure mechanics of the storage formation, and could cause failure that also might jeopardize the surrounding seal. We have identified five settings for the encountered fracture systems (Ogata et al., 2014):

1. Joints (mode I) – commonly associated with tectonic forces, compaction or decompaction from burial/uplift or mineral reactions, and fluid pressure-driven failure;
2. Fault core fractures – found as extensive slip-surfaces (shear fractures, mode II) interlinked with minor fractures, or in lenses of wall rock or fault rock hosted by the core of overall semi-penetrative strain;
3. Fault damage zone fractures (modes I and II) – networks of fractures related to discrete fault strain outside of the fault core;
4. Fault-tip process zone fractures – fringes of fractures found at the tip of faults;
5. Fold-crest fractures (mode I) – linked to outer arch stretching of fold hinges.

One of the cases specifically addressing CO_2 storage is the natural subsurface CO_2 plumes of Utah, US, which have received significant attention (Dockrill and Shipton, 2010; Kampman et al., 2013). A recent research well into a fault damage zone (with full coring of the stacked sequence of reservoirs and caprocks and sampling of fluids allowing mapping of CO_2 saturation) suggests that fluid over-pressure is important for the current leakage (Kampman et al., 2013). Expanding on these observations, Ogata et al. (2012; 2014) mapped exhumed reservoir-seal systems of Utah, showing that enhanced fracturing characterized by closely-spaced, sub-parallel fracture networks (i.e. fracture corridors) acted as fluid pathways (bleaching pathways) in both permeable sandstone and tight lithologies (Figure 4).

Field observations of deformed porous sandstones have shown that deformation bands are very 'selective' in the sense that they only form in sandstone layers with a certain range of properties. Among the properties that are seen to affect deformation localization and growth are porosity, permeability, cementation, grain size, sorting and mineralogy. Most of these factors change throughout the lifespan of sandstone as a function of stress and temperature.

Field studies on cemented and non-cemented Navajo Sandstones (Utah) show that cementation has a significant effect on permeability and mechanical properties of sandstone (Alikarami et al., 2013). In the damage zone of the fault within the non-cemented Navajo Sandstone in Cache Valley, zones of deformation bands show the highest strength and Young's modulus and the lowest permeability. Open fractures in the cemented Navajo Sandstone in the San Rafael Swell may enhance fluid flow and CO_2-leakage in this reservoir (Alikarami et al., 2013; Skurtveit et al., 2014b).

The localization of deformation bands leads to faulting through the formation of a through-going slip surface, while the surrounding deformation bands constitute the damage zone. Slip surfaces propagate through low-porosity sandstones and other lithologies to form faults that can grow to seismic-scale structures. Skurtveit et al., (2014b) report normal faults formed due to the propagation of cataclastic bands in the Navajo and Page formations in the San Rafael Swell. The cataclastic bands were later overprinted by fractures (open and cemented (veins)). The calcite cementation in the veins could be attributed to a CO_2-bearing fluid along fractures. This suggests that faults and their surrounding damage zones can change from barriers to conduit depending on the dominant deformation mechanism involved.

Among the petrophysical properties of faulted sandstone, porosity and permeability have been the focus of most researchers (Antonellini and Aydin, 1994; Fisher and Knipe, 1998, 2001; Sternlof et al., 2004), while capillary pressure has received less attention (Torabi et al., 2013).

The capillary trapping of CO_2 in reservoir rocks might be enhanced in fault-related rocks through compaction and grain crushing (Torabi et al., 2013). A correlation can be

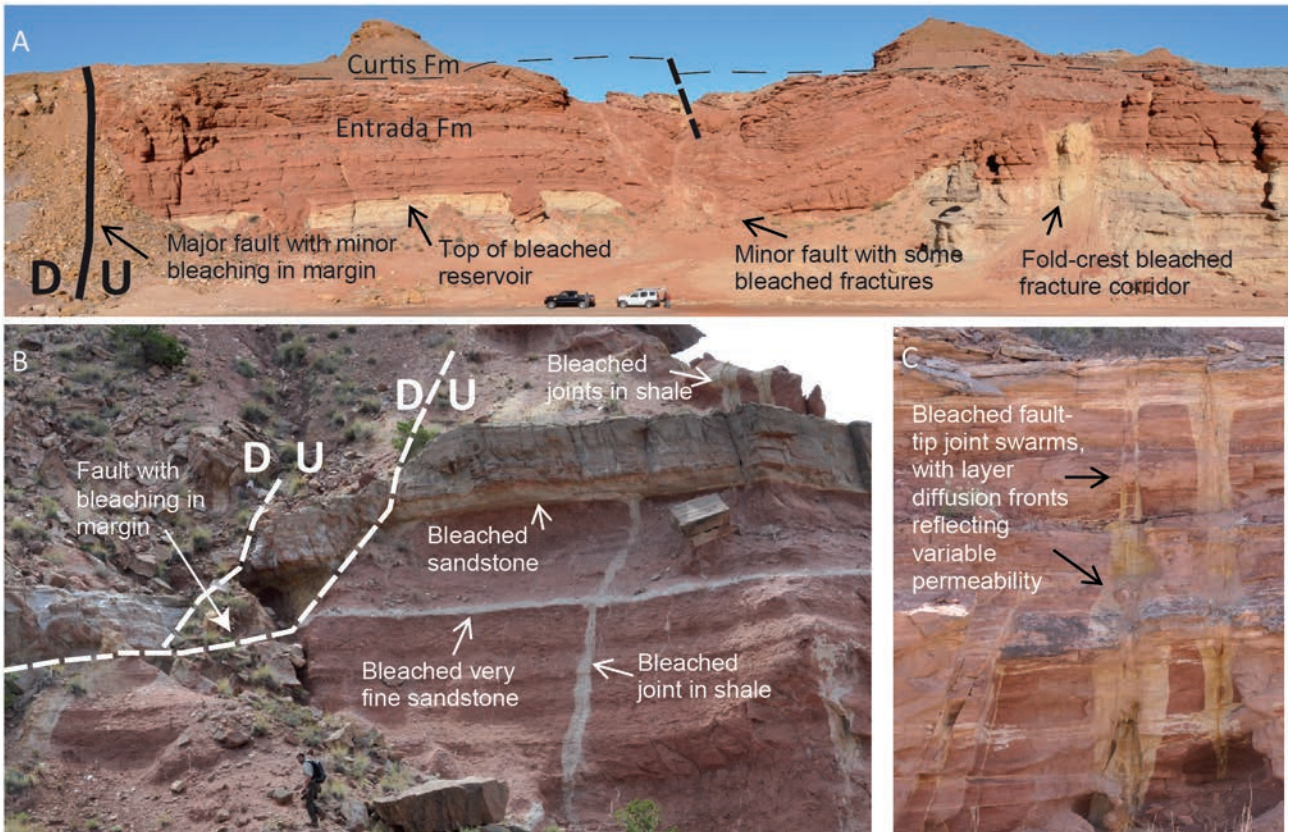

Figure 4 *a) Salt Wash Graben case study. The photograph shows the northern, major fault of the Salt Wash Graben (left, south) and the northern footwall (view to the NW). The lower part of the Entrada Fm offers a bleached out reservoir (see C for details). b) Chimney Rock case study of the Entrada Fm, with 4.5 m offset normal fault cutting a medium grained sandstone layer. Note bleaching along the fault and along joints in shale of the footwall as well as in the interlayers of sandstone in shale. c) Salt Wash Graben case study, showing a fault-tip joint swarm with bleaching. The variable width of bleaching into sandstone and siltstone suggests that the reducing fluid penetrated deeper into more permeable units.*

found between the degree of consolidation, the dominant deformation mechanism, and the sealing capacity of the fault rocks (Torabi, 2012; Figure 5). The damage zone of faults in poorly consolidated, moderately consolidated and consolidated sandstones is dominated by deformation bands leading to lower permeability and higher capillary pressure, which may cause trapping of a higher column of CO_2. While it would be the opposite for the damage zone of well-consolidated and cemented sandstones which are dominated by fractures, (Figure 5). Although permeability and porosity are reduced in the damage zone of faults formed in poorly consolidated sandstones with high content of clay and phyllosilicate, the slip surfaces are characterized by lower capillary pressure (Figure 5) and seem to act as conduits in these rocks.

Analogue experiments – investigation of fault linking in mechanically stratified sequences

Multiple levels of fault decoupling due to contrasting mechanical strength are commonly reported for extensional fault systems (Withjack and Callaway, 2000; Wilson et al., 2013). Such situations occur particularly where strata-bound units of mechanically weak rock units, such as salt or mudstone, are parts of the lithostratigraphic sequence (Withjack and Callaway, 2000; Wilson et al., 2013) but can also be promoted by contrasting compaction and fluid pressure.

One fault complex of this kind is the Ringvassøy-Loppa Fault Complex (Gabrielsen, 1984; Gabrielsen et al., 1997; Faleide et al., 1993) of the Barents Sea that contributes to constraining the Snøhvit Field to the west (Figure 3).This fault complex is characterized by a late Palaeozoic initiation and was reactivated in several stages in the Mesozoic-Cenozoic (Gabrielsen et al., 1997; Faleide et al., 1993). This resulted in a complex geometry, seemingly with multiple levels of dislocations as interpreted from reflection seismic data (Gabrielsen, 1984).

The three series of experiments presented below demonstrate the significant influence that mechanical stratification can have on the structuring of a lithostratigraphic sequence, which is subjected to multi-stage deformation. The experiments include:

- Stratified sand not interlayered by silicon putty layers;
- Stratified sand separated by a layer of silicone putty;
- Adding an additional (second) silicon putty layer;

In the experiment where an additional (second) silicon putty layer was added, three levels of faulting occurred. The fault system formed in between the two silicon layers consisted of

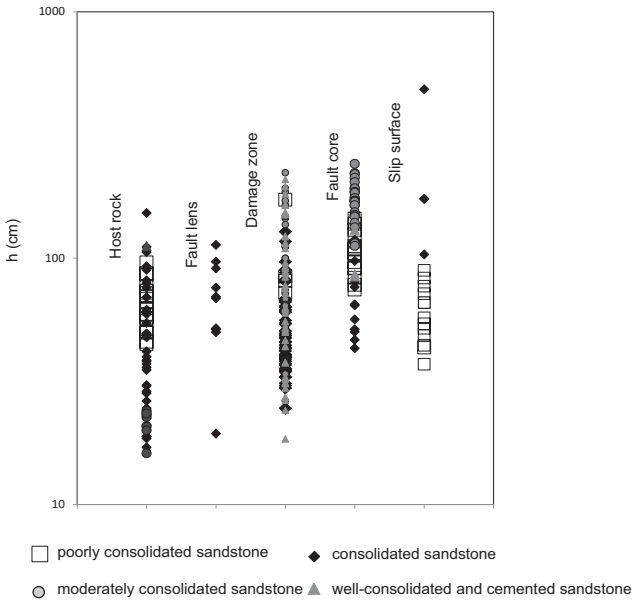

Figure 5 *Possible sealed column height of CO_2 due to capillary effect for undeformed (host rock) and different types of fault rocks with different degrees of consolidation; calculations of h were performed using the algorithm (approach B) suggested by Torabi et al. (2013). The classification of sandstones is based on their host rock porosity, degree of cementation and consolidation, and burial depth at the time deformation.*

a symmetric graben. In these cases, each layer above a silicon putty layer developed its specific, intra-formational fault system. This nicely explains the contrasting fault patterns and the depth-dependent extension at several different levels as seen in the Ringvassøy-Loppa Fault Complex of the Barents Sea. In some cases where the uppermost layer was significantly stronger than its substratum, wide, coherent blocks of the upper-layer sand sequences slide across the graben edge, rotating towards the graben axis, resulting in faults with reverse geometry in the central graben (Figure 6). This is similar to analogue experimental results obtained by Dooley et al. (2003) and Withjack and Callaway (2000). Such configurations are common on the mid-Norwegian continental shelf for instance the Mikkel structure (Withjack and Callaway, 2000) and the Revfallet Fault Complex (Dooley et al., 2003). Reverse faults are also promoted by strong contrasts in mechanical stiffness where the stronger layer is the deepest (Horsfield, 1977).

This study shows that even for long-lived faults that are positioned above deep-seated (basement) locations of instability (faults), linkage can be mechanically discontinued in beds of high plasticity (e.g. unconsolidated mudstones and salt-dominated evaporitic sequences) in the vertical dimension. Such beds may represent baffles to fluid communication, which may prevent unwanted leakage of CO_2 from deeply buried reservoir units, but which could also constrain efficient injection of CO_2.

Triaxial experiments on sand and sandstone

Triaxial experiments investigating the localization of deformation for various consolidation stresses and initial porosity of sandstone/sand were performed in the rock mechanics laboratory facility of Norwegian Geotechnical Institute in Oslo. Results from high-pressure triaxial testing were used to study deformation mechanisms involved during shear-enhanced compaction in deformation bands and controlling parameters for yield stress at varying confining pressure for sandstone/sand with contrasting grain size, porosity, and packing. Sands from the Boncavaï quarry in France with different modes of grain-packing were used: 1) natural coarse-grained sandstone (2) densely packed fine-grained sand and (3) loosely packed fine-grained sand (Skurtveit et al., 2013). Only results from tests on densely packed fine-grained sand are presented here (Figure 7).

The experimental work on shear-enhanced compaction (Skurtveit et al., 2013, 2014a) has provided insight into some critical aspects of shear-enhanced compaction in poorly consolidated sandstone; (1) the large inelastic deformation observed during testing and (2) a change in deformation mechanisms from grain rearrangement into grain fracturing and crushing. The combined effect of both inelastic and elastic deformation during compaction is expressed as porosity reduction. The results are presented as elliptical end-caps (Cap surfaces) for given porosities for densely packed fine sand (Figure 7a). These show that the onset of shear-enhanced compaction does not occur in the form of a single end-cap as observed for consolidated sandstone (e.g. Wong and Baud, 2012). Rather, it relates to the observed porosity reduction during increasing total mean stress and differential stress, mapping out elliptical end-caps increasing in size during compaction at higher confining pressures.

The observed onset of grain fracturing at effective pressure of 5-10 MPa (Figure 7b) supports the idea that cataclastic shear-enhanced compaction bands might have been formed at shallow burial depth in the field. Comparison of laboratory tests with field observations (Skurtveit et al., 2014a) show that grain size and compaction behaviour may control the selective formation of shear-enhanced compaction bands in sands from the Boncavaï quarry.

Well-defined localization of shear bands was not observed in the tests. The grain-crushing, as seen in the sample by final strain, was distributed over a wider area of the sample (Figure 7c).

Triaxial experiments on sand inside an x-ray scanner

Two different sands were tested in this work: Hostun HN31 sand (angular, D_{50}= 338 μm) and Ottawa 50-70 sand (rounded; D_{50}= 310 μm). A series of triaxial tests on small specimens (22 mm height and 11 mm diameter) of dry sands at confining pressures ranging from 100 kPa to 7000 kPa (7 MPa) were performed at the Laboratoire 3SR applying simultaneous *in-situ* x-ray scanning (Alikarami et al., 2014). Among the performed tests, only the tests at the lowest (100 kPa) and highest (7000 kPa) confining pressure are presented here.

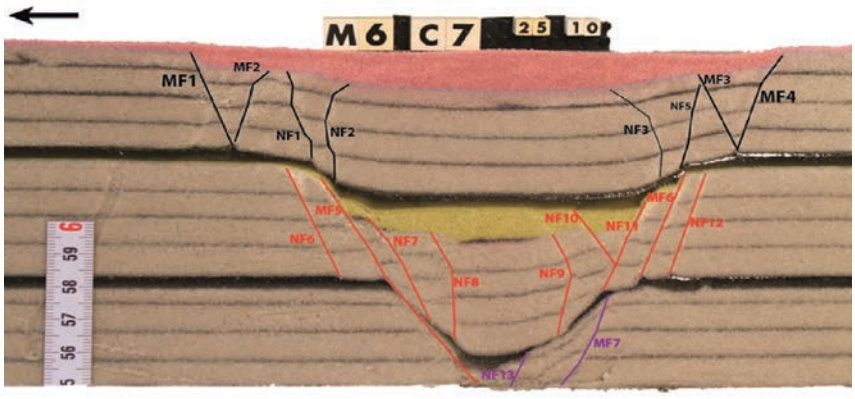

Figure 6 *Experiment where an additional (second) silicon putty layer was added, three levels of faulting occurred.*

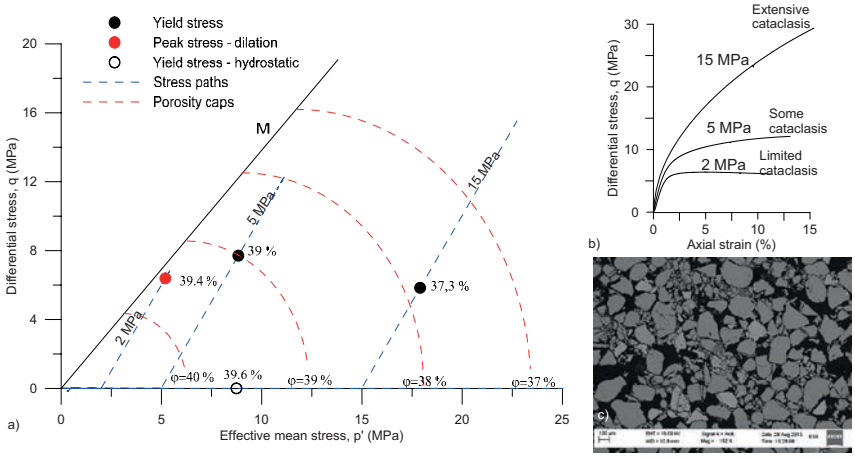

Figure 7 *a) Porosity at yield stress in axial compression tests compared with yield caps calculated from hydrostatic loading of densely packed fine sand (Skurtveit et al., 2013). b) Stress-strain curve for the 2, 5 and 15 MPa stress paths showing the variation in deformation and description of observed cataclasis. c) Post-test SEM image for axial compression test at 5 MPa confining stress showing cataclasis distributed within the sample.*

The image analysis techniques were used to make micro-scale measurements (porosity and strain) on the various 3D tomography-images during loading (Alikarami et al., 2014).

At 100 kPa both sands exhibit a clear stress peak, which is followed by a plateau approaching a residual stress state. It is anticipated that, strain softening follows strain hardening while the specimen dilated. With increasing confining pressure, the trend is to have a less marked stress peak and less dilatancy – Hostun sands appears to be more sensitive to confining pressure (Figures 8a and b).

The porosity distribution maps obtained for some key steps during the triaxial shearing of Ottawa sand specimens show that at 100 kPa confinement, a dilatant shear band develops early in the test – around the peak stress, (Figure 9). The mechanism at 7000 kPa confinement is different: first a dilatant shear band is visible at 12.9% but by the end of the test, a compactive shear band forms. This band is consistent in space with the zone of crushed material (Figure 9).

Image correlation of vertical sections (DIC) results in volumetric and deviatoric strains for some selected increments of tests. DIC for Ottawa sand showed that over the peak, in contrast to porosity measurements, the volumetric strain in the bands either disappeared (for the test at lower confinement) or became compactive possibly due to grain breakage (at higher confinement). The shear strain fields show that in both cases the band becomes thinner after the peak.

The porosity map of specimen HNEA01 shows a shear band that becomes more dilatant with increasing shortening (Figure 10). Specimen HHEA01 which was tested at 7000 kPa confinement deforms with a progressive and distributed reduction in porosity, which is related to grain crushing in the sample (Figure 10). Based on DIC results for Hostun sands, at 100 kPa confinement strain localizes in a wide band and then gets narrower with increasing axial shortening. At 7000 kPa, the shear strain concentrates in a similar fashion, a shear band eventually forms.

Hydro-mechanical modelling of strain localization in porous sandstone

To better understand the influence of strain localization on the hydro-mechanical behaviour of porous rocks, this numerical study is focused on the material response of fully saturated samples. The kinematic of the skeleton is enriched using the second gradient theory (Collin et al., 2006) so that an internal length can be introduced in the modelling and the appearance of possible localized deformations can be properly described. To obtain numerical results with the finite element method, the weak formulation of equilibrium and mass balance fluid equations are enforced.

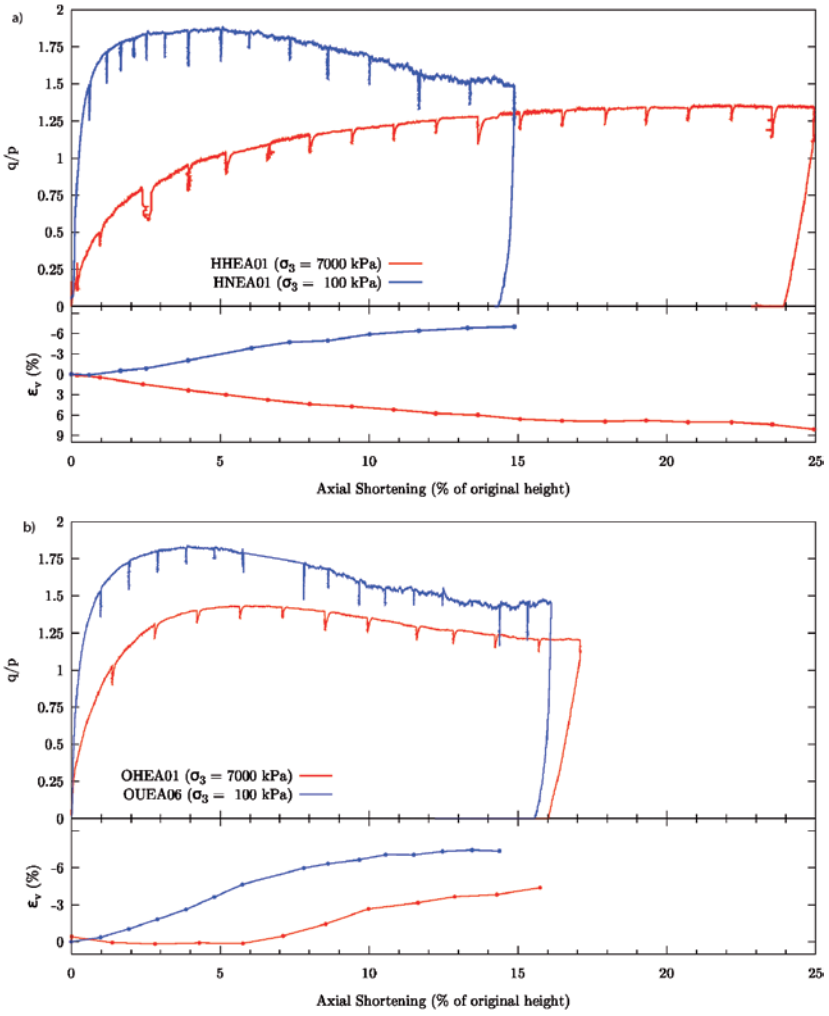

Figure 8 *Deviatoric stress normalized by the mean stress (q/p) vs. axial shortening (top) and volumetric strain vs. axial shortening (bottom) for triaxial compressions tests on Hostun sand (a) and on Ottawa sand (b).*

In this study, the hydromechanical behaviour of high porosity rocks is investigated in the case of biaxial tests with no confining pressure. A rectangular geometry (25 mm x 50 mm) retaining the same size of the sample used in a true triaxial apparatus (see Bésuelle and Hall, 2011) was utilized including 3200 finite elements. At the top of the specimen a strain ($\overline{u}_y = 3mm$) is enforced at different loading rates. The hydromechanical parameters used in the computations are presented in the Table 1.

Cohesion c and friction angle φ represent the hardening/softening variables as a function of the Von Mises equivalent plastic strain distribution, ε_{eq}^{p}. A hyperbolic variation of the friction angle and cohesion between initial (φ_i and c_i) and final values (φ_f and c_f) is considered in the hardening rule (Equation 1) of this constitutive equation. In particular, hardening on friction angle and softening on cohesion are taken into account to model the behaviour of the skeleton.

$$\begin{pmatrix} \varphi \\ c \end{pmatrix} = \begin{pmatrix} \varphi_i + \left(\dfrac{\varphi_f - \varphi_i}{\beta_\varphi + \varepsilon_{eq}^{p}} \right) \varepsilon_{eq}^{p} \\ c_i + \left(\dfrac{c_f - c_i}{\beta_c + \varepsilon_{eq}^{p}} \right) \varepsilon_{eq}^{p} \end{pmatrix} \quad (1)$$

β_c and $\beta\varphi$ represent the parameters of the hardening law indicating the rate of the hardening process. In the interest of simplicity, only one parameter (namely D, the second gradient parameter) is used following the approach of Bésuelle et al. (2006). The loading rate varies in the range from $\dot{\overline{u}}_y$ = 1 mm/1h to $\dot{\overline{u}}_y$ = 1 mm/3.6s. Since the excess of the pore fluid pressure for the case in which $\dot{\overline{u}}_y$ = 1 mm/1h is close to zero ($\Delta p_w \approx 0$), this case can be considered locally drained (not shown here).

To describe the global behaviour of the sample under the prescribed boundary conditions, the total vertical reaction R, defined as a sum of all nodal reactions at the bottom of the sample, is plotted in Figure 11 as a function of the normalized time t/T.

Before the appearance of strain localization, all the numerical tests are characterized by the same behaviour that shows an initial elastic phase and then, before the strain localization, the accumulation of plastic strain. After the onset of localization, the curves of Figure 11 differ by the time at which the shear bands are triggered, i.e. for faster loading rates, the shear bands appear sooner due to the increasing of the excess pore pressure in the

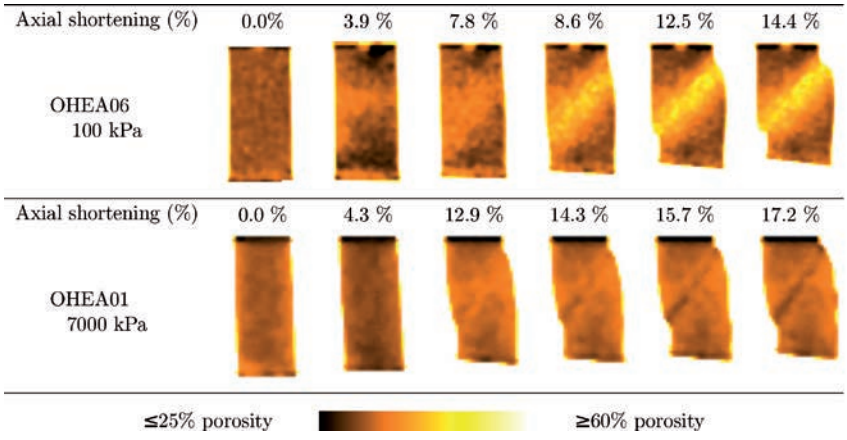

Figure 9 *Porosity maps of some selected states of two specimens of Ottawa sand during shearing, modified after Alikarami et al., 2014.*

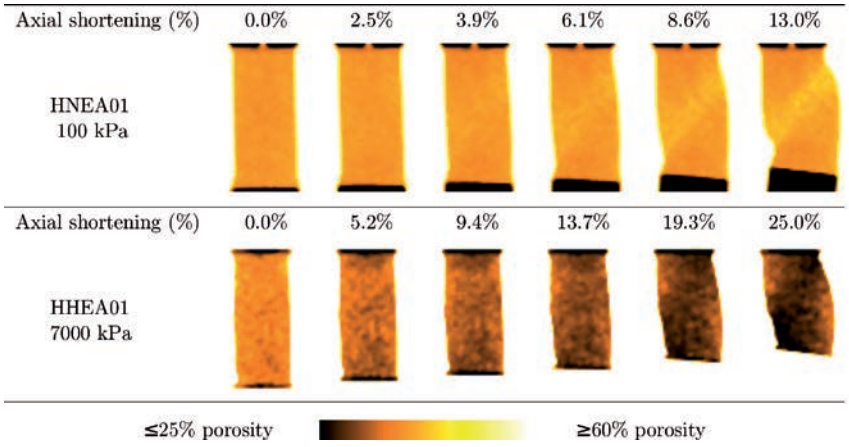

Figure 10 *Porosity maps of some selected states of two specimens of Hostun sand during shearing, modified after Alikarami et al., 2014.*

specimen core. The corresponding localization phenomena are characterized by different configurations (*conjugated* and *crossed shear bands*). In order to identify these configurations, the index loading and the equivalent plastic strain ε_{eq}^{p} are considered. The loading index is graphically represented as follows: if a Gauss point undergoes plastic loading, a small blue square is plotted, otherwise (in the case of elastic unloading or reloading of the Gauss point), a small yellow square is plotted. The loading index is plotted in Figure 12 for all cases at the normalized time t/T corresponding to the triggering shear bands time.

As a consequence of the increasing loading rates, the overpressures inside the specimen tend to increase. Since in the selected model the plastic strains are computed by the plastic potential characterized by a given dilatancy ψ, the accumulation of shear strain ε_{eq}^{p} involves extensive volumetric plastic strain. This aspect explains the development of negative pore pressure p_w that, for high value of p_w could trigger cavitation (Figure 13). In this study, cavitation is not modelled.

Discussion and conclusions

The results summarized here illustrate the improved understanding of processes and products of deformation in porous sandstone at different scales. This is important in forecasting

Parameters of the fluid and solid phase	
Young's Modulus E [MPa]	12300
Poisson's ratio v [-]	0.215
Initial cohesion c_i [MPa]	32.5
Final cohesion c_f [MPa]	9.6
Softening parameters β_c [-]	0.03
Hardening parameters β_φ [-]	0.00067
Initial friction angle φ_i [°]	4
Final friction angle φ_f [°]	21
Dilation angle ψ [°]	18
Initial porosity ϕ [-]	0.26
Intrinsic permeability κ [m^2]	5 * 10^{-10}
Parameters of the fluid and solid phase	
Water specific mass ϱ^w [kg/m^3]	1000
Water dynamic viscosity μ [Pa.s]	1.0^{-4}
Water compressibilty $1/k^w$ [Mpa^{-1}]	1.0^{-4}
Solid specific mass ϱ^s [kg/m^3]	2026
Parameters of the second gradient model	
Second gradient parameter [N] D	3

Table 1 *Parameters of the porous medium utilized in the numerical modelling.*

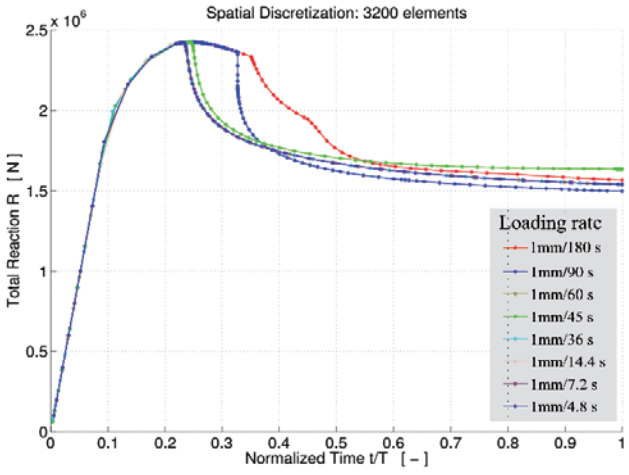

Figure 11 Total vertical reaction R: global behavior of the sample.

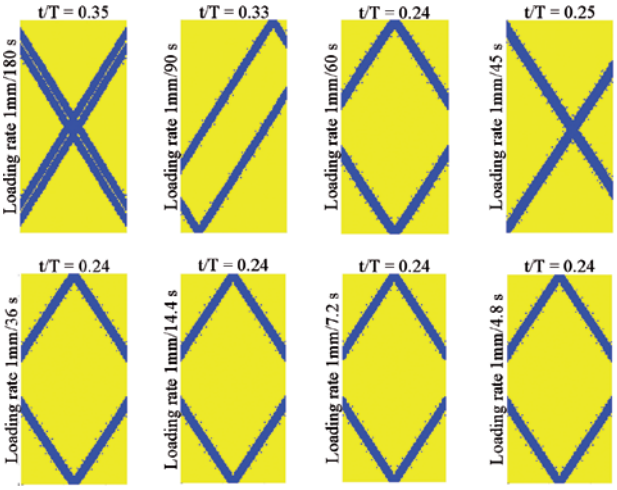

Figure 12 Loading index at the triggered time of shear bands.

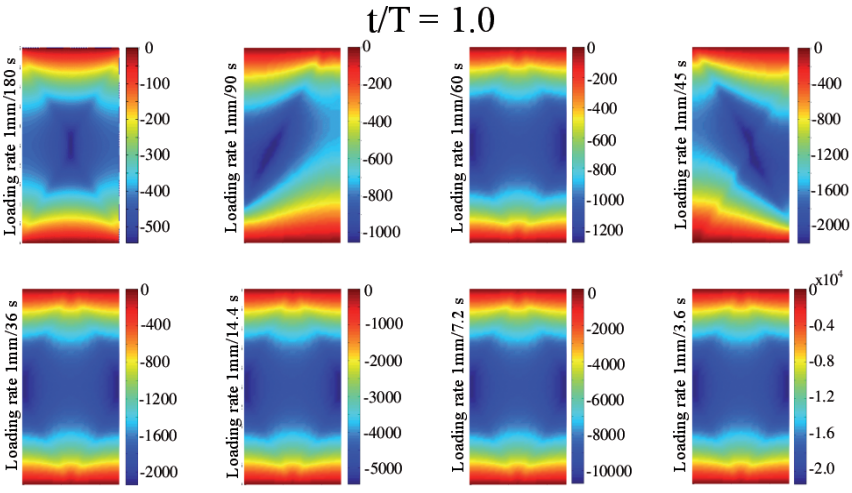

Figure 13 Fluid pore pressure at the end of the loading path (t/T=1). The legend colours are referred to Pa.

the distribution and impact of faults on reservoir/aquifer performance and sealing properties, optimizing planning and the choice of reservoir/aquifer for CO_2 storage.

We have investigated faults and their effects on distribution of CO_2 in Snøhvit field by integrating seismic attributes and 4D anomalies. Using appropriate fault attributes helped to visualize faults that were otherwise hidden in the seismic. The complexity of fault systems in areas of multiple reactivations was studied by field study and analogue mechanical experiments. The main finding is that strong mechanical contrasts in sediment sequences are likely to cause fault geometries that prevent homogeneous upward migration conditions for faults with regional significance. This was supported by analysis of the condition for strain localization in porous sandstone and sand through triaxial experiments demonstrating the importance of confining pressure, relative density, sorting, grain size and grain shape (angularity), as shown in Figure 7 and Figures 8-10. Microstructural imaging of the experiments revealed that grain breakage (crushing) is an important deformation mechanism in poorly consolidated sandstone and sand for confining pressures ranging from 4 MPa and higher. The effect of angularity of sand grains on the degree of grain crushing and deformation pattern is emphasized in triaxial experiments run by utilizing CT-scan images and DIC results. Our numerical modelling reveals that loading rates and pore pressure increase affect the localization and configuration of the observed shear bands. These new insights into deformation mechanisms and kinematics, which are influenced by the applied loading and the petrophysical properties of granular material, illustrate the factors needed for prediction of strain localization and communication within highly porous sandstone reservoirs that are a major target for current and future CO_2 storage sites.

Some of the main conclusions of this study are:

- Geological field measurements of permeability and strength of undeformed and deformed sandstones can be used in forecasting the behaviour of these rocks when subjected to stress change due to pore-pressure increase as a result of CO_2 injection.

- Pre-deformation cementation increases the strength of the host rock and therefore promotes fracturing upon deformation. This will have a positive effect on permeability and conductivity of such rocks.
- Cataclastic bands that are overprinted by open fractures due to a change in stress conditions could change them from being barriers to conduits for CO_2.
- Deformation mechanisms and kinematics of deformation bands change with increasing confining pressure (in the triaxial experiments).
- Sorting and initial porosity affect the sandstone behaviour under compaction.
- Angularity of sand grains influences the strain localization process and the degree of grain breakage and kinematics in the localized bands.
- Analogue fault models improve understanding of the kinematic and possible reactivation scenarios of faults in the Hammerfest basin of the Barents Sea.

Acknowledgement

This study is part of a consortium R&D project 207806 (IMPACT Project) based at Uni Research CIPR and funded by the CLIMIT Programme at the Research Council of Norway and Statoil ASA. We would like to acknowledge the sponsors of the project for their financial and scientific supports. We would also like to thank the Snøhvit Production Licence for permission to use site data.

References

Alikarami, R., Torabi, A., Kolyukhin, D. and Skurtveit, E. [2013] Geostatistical relationships between mechanical and petrophysical properties of deformed sandstone. *International Journal of Rock Mechanics and Mining Sciences*, **63**, 27-38.

Alikarami, R. Ando, E., Gkiousas-Kapnisis, M., Torabi, A. and Viggiani, G. [2014] Strain localisation and grain breakage in sand under shearing at high mean stress: insights from in situ X-ray tomography. *Acta Geotechnica*, DOI: 10.1007/s11440-014-0364-6.

Antonellini, M. and Aydin, A. [1994] Effect of faulting on fluid flow in porous sandstones: Petrophysical properties. *AAPG Bulletin*, **78**, 355–377.

Baines, S.J. and Worden, R.H. [2004] The long-term fate of CO_2 in the subsurface: natural analogues for CO_2 storage. In: Baines, S.J. and Worden, R.H. (Eds.) *Geological Storage of Carbon Dioxide, Geological Society of London Special Publication*, **233**, 59-85.

Bésuelle, P. and Rudnicki, J.W. [2004] Localizations, shear bands and compaction bands. In: Guéguen, Y. and Boutéca, M. (Eds.) *Mechanics of Fluid-saturated Rocks*, 219-321.

Bésuelle, P., Chambon, R. and Collin, F. [2006] Switching deformation modes in postlocalization solutions with quasi-brittle material. *Mechanics of materials and structures*, **1** (7), 1115–1134.

Bésuelle, P. and Hall, S. [2011] Characterization of strain localization in a porous rock in plane strain condition using a new true-triaxial test apparatus. In: *Advances in Bifurcation and Degradation in Geomaterials*, Laboratoire 3S-R, 345–352.

Caine, J.S., Evans, J.P. and Forster, C.B. [1996] Fault zone architecture and permeability structure. *Geology*, **24**, 1025–1028.

Chiaramonte, L., White, J. A., and Trainor-Guitton, W. [2014]. Probabilistic Geomechanical Analysis of Compartmentalization at the Snøhvit CO_2 Sequestration Project. *Journal of Geophysical Research: Solid Earth*. 10.1002/2014JB011376.

Chopra, S. and Marfurt, K.J. [2008] Seismic Attributes for Prospect Identification and Reservoir Characterization. *SEG Geophysical Developments Series*, **11**.

Collin F., Chambon, R. and Charlier, R. [2006] A finite element method for poro mechanical modelling of geotechnical problems using local second gradient models. *International Journal for Numerical Methods in Engineering,* **65**, 1749–1772.

Couples, G. [2005] Seals: the role of geomechanics. In: Boult, P. and Kaldt, J. (Eds.) Evaluating fault and cap rock seals, *American Association of Petroleum Geologists*, Heiberg Series, **3**, 87-108.

Dockrill, B. and Shipton, Z.K. [2010] Structural controls on leakage from a natural CO_2 geologic storage site: Central Utah, U.S.A. *Journal of Structural Geology*, **32** (11), 1768-1782.

Dooley, T., McClay, K.R. and Pascoe, R. [2003] 3D analogue models of variable displacement extensional faults: applications to the Revfallet Fault system, offshore mid-Norway. *Geological Society, London, Special Publications*, **212** (1), 151-167.

Faleide, J.I., Vågnes, E. and Gudlaugsson, S.T. [1993] Late Mesozoic – Cenozoic evolution of the south-western Barents Sea in a regional rift-shear tectonic setting. *Marine and Petroelum Geology*, **10**, 186-214.

Fisher, Q.J., and Knipe, R.J. [1998] Fault sealing processes insiliciclastic sediments. In: Jones, G., Fisher, Q.J. and Knipe, R.J., (Eds.) *Faulting and fault sealing in hydrocarbon reservoirs*, Geological Society London, Special Publication, **147**, 117–134.

Fisher, Q.J. and Knipe, R.J. [2001] The permeability of faults within siliciclastic petroleum reservoirs of the North Sea and Norwegian Continental Shelf. *Marine and Petroleum Geology*, **18**, 1063–1081, DOI: 10.1016/S0264-8172(01)00042-3.

Fossen, H., Schultz, R.A., Mair, K. and Shipton, Z. [2007] Deformation bands in sandstones – A review. *Journal of Geological Society* (London), **164**, 755–769, doi: 10.1144/0016-76492006-036.

Gabrielsen, R.H. [1984] Long-lived fault zones and their influence on the development of the southwestern Barents Sea. *Journal of the Geological Society of London*, **141** (4), 651–662.

Gabrielsen, R.H., Grunnaleite, I. and Rasmussen, E. [1997] Cretaceous and Tertiary inversion in the Bjørnøyrenna Fault Complex, south-western Barents Sea. *Marine and Petroleum Geology*, **14** (2), 165-178.

Gray, D., Anderson, P., Logel, J., Schmidt, D. and Schmid, R. [2012] Estimation of stress and geomechanical properties using 3D seismic data. *First Break*, **30** (3), 59–68.

Grude, S., Dvorkin, J., Clark, A., Vanorio, T. and Landrø, M. [2013] Pressure effects caused by CO_2 injection in the Snøhvit field. *First Break*, **31**, 99–101.

Halland, E.K., Johansen, W.T. and Riis, F. [2011] *CO_2 storage atlas: Norwegian North Sea*. Norwegian Petroleum Directorate, Stavanger. Accessed at: http://www.npd.no.

Hansen, O., Eiken, O., Østmo, S., Johansen, R. I. and Smith A. [2011] Monitoring CO_2 injection into a fluvial brine-filled sandstone

formation at the Snøhvit field, Barent Sea. *SEG Annual Meeting*, Expanded Abstracts.

Hansen, O., Gilding, D., Nazarian, B., Osdal, B., Ringrose, P., Kristoffersen, J-B., Eiken, O., Hansen, H. [2013] Snøhvit: The history of injecting and storing 1 Mt CO_2 in the fluvial Tubåen Fm. *Energy Procedia*, **37**, 3565–357.

Henderson, J. [2012] Geological Expression: data driven–interpreter guided approach to seismic interpretation. *First Break*, **30**, 73–78.

Hildebrand, A. and Kroos, B.M. [2003] CO_2 migration processes in argillaceous rocks pressure-driven volume flow and diffusion. *Journal of Geochemical Exploration*, **78/79**, 169–172.

Horsfield, W.T. [1977] An experimental approach to basement-controlled faulting. *Geologie en Mijbouw*, **56** (4), 3634-370.

Hovland, A.B. [2013] *Detailed structural imaging of Snøhvit Field using seismic attribute analysis*. Master thesis, University of Bergen.

Iding, M. and Ringrose, P. [2010] Evaluating the impact of fractures on the performance of the In Salah CO_2 storage site. *International Journal of Greenhouse Gas Control*, **4**, 242–248.

Kampman, N., Maskell, A., Bickle, M.J., Evans, J.P., Schaller, M., Purser, G., Zhou, Z., Gattacceca, J., Peitre, E.S., Rochelle, C.A., Ballentine, C.J., and Busch, A. [2013] Scientific drilling and downhole fluid sampling of a natural CO_2 reservoir, Green River, Utah. *Scientific Drilling*, **16**, 33–43, DOI:10.5194/sd-16-33-2013.

Ogata, K., Senger, K., Braathen, A., Tveranger, J., Petrie, E. and Evans, J. [2012] Fracture-related fluid flow in sandstone reservoirs: insights from outcrop analogues of south-eastern Utah. *Third EAGE CO_2 Geological Storage Workshop*, Extended Abstracts.

Ogata, K., Senger, K., Braathen, A., and Tveranger, J. [2014] Fracture corridors as seal-bypass systems in siliciclastic reservoir-cap-rock successions: fieldbased insights from the Jurassic Entrada Formation (SE Utah, USA). *Journal of Structural Geology*, **66**, 162-187.

Rutqvist, J. [2012] The Geomechanics of CO_2 Storage in Deep Sedimentary Formations. *Geotechnical and Geological Engineering*, **30** (3), 525-551.

Shipton, Z.K. and Cowie, P.A. [2003] A conceptual model for the origin of fault damage zone structures in highporosity sandstone. *Journal of Structural Geology*, **25**, 333–345, doi:10.1016/S0191-8141(02)00037-8.

Skurtveit, E., Torabi, A., Gabrielsen, R.H., and Zoback, M.D. [2013] Experimental investigation of deformation mechanisms during shear-enhanced compaction in poorly consolidated sandstone and sand. *Journal of Geophysical Research: Solid Earth*, **118** (8), 4083–4100.

Skurtveit E., Ballas, G., Fossen H., Torabi, A., Soliva R. and Peyret, M. [2014a] Sand textural control on shear-enhanced compaction bands in poorly-lithified sandstone. *Journal of Geological Resource and Engineering*, **2** (2), 115–130.

Skurtveit, E., Torabi, A., Alikarami, R. and Braathen, A. [2014b] Fault baffle to conduit developments: reactivation and calcite cementation of deformation band fault in aeolian sandstone. *Petroleum Geoscience*, doi:10.1144/petgeo2014-031.

Sternlof, K.R., Chapin J.R., Pollard, D.D. and Durlofsky, L.J. [2004] Permeability effects of deformation band arrays in sandstone. *AAPG Bulletin*, **88** (9), 1315–29.

Torabi, A. [2012] Effect of burial depth on deformation and storage capacity of sandstone reservoirs. *Third EAGE CO_2 Geological Storage Workshop*, Extended Abstracts.

Torabi, A., Fossen, H. and Braathen, A. [2013] Insights into petrophysical properties of deformed sandstone reservoirs, *AAPG Bulletin*, **97** (4), 619–637.

Yielding, G., Lykakis, N. and Underhill, J.R. [2011] The role of stratigraphic juxtaposition for seal integrity in proven fault-bound traps of the Southern North Sea. *Petroleum Geoscience*, **17**, 193–203, doi: 10:1144/1354-0793/10-026.

Wilson, P., Elliott, G.M., Gawthorpe, R.L., Jackson, C.A.L., Michelsen, L. and Sharp, I.R. [2013] Geometry and segmentation of an evaporate-detached normal fault array: 3D seismic analysis of the southern Bremstein Fault Complex, offshore mid-Norway. *Journal Of Structural Geology*, **51**, 74–91.

Withjack, M.O. and Callaway, S. [2000] Active normal faulting beneath a salt layer: an experimental study of deformation patterns in the cover sequence. *AAPG bulletin*, ***84*** (5), 627–651.

Wong, T.F. and Baud, P. [2012] The brittle-ductile transition in porous rock: A review. *Journal of Structural Geology*, **44**, 25–53.

Zweigel, P., Arts, R., Lothe, A.E. and Lindberg, E.B.C. [2004] Reservoir geology of the Utsira Formation at the first industrial-scale underground CO_2 storage site (Sleipner area, North Sea). In: Baines, S.J. and Worden, R.H. (Eds.) *Geological Storage of Carbon Dioxide*, Geological Society of London Special Publication, 233, 165–180.